Article

Neuron

Glutamate-Induced AMPA Receptor Desensitization Increases Their Mobility and Modulates Short-Term Plasticity through Unbinding from Stargazin

Highlights

- Glutamate increases AMPA receptor diffusion in a conformation-dependent manner
- Desensitized AMPAR diffuse faster than closed-resting or open ones
- Preventing AMPAR-stargazin dissociation blocks glutamate-induced AMPAR diffusion
- AMPAR-stargazin unbinding speeds recovery from synaptic short-term depression

Authors

Audrey Constals, Andrew C. Penn, ..., Eric Hosy, Daniel Choquet

Correspondence

eric.hosy@u-bordeaux.fr (E.H.), daniel.choquet@u-bordeaux.fr (D.C.)

In Brief

Constals et al. use single-molecule tracking to show that desensitized AMPA receptors diffuse faster than closed-resting or open ones through unbinding from stargazin. This allows AMPA receptor diffusion to accelerate recovery from short-term synaptic depression.

Constals et al., 2015, Neuron *85*, 1–17
February 18, 2015
http://dx.doi.org/10.1016/j.neuron.2015.01.012

CellPress

Neuron
Article

Glutamate-Induced AMPA Receptor Desensitization Increases Their Mobility and Modulates Short-Term Plasticity through Unbinding from Stargazin

Audrey Constals,[1,2] Andrew C. Penn,[1,2] Benjamin Compans,[1,2] Estelle Toulmé,[1,2] Amandine Phillipat,[1,2] Sébastien Marais,[3] Natacha Retailleau,[1,2] Anne-Sophie Hafner,[1,2] Françoise Coussen,[1,2] Eric Hosy,[1,2,4,*] and Daniel Choquet[1,2,3,4,*]

[1]University of Bordeaux, Interdisciplinary Institute for Neuroscience, UMR 5297, F-33000 Bordeaux, France
[2]CNRS, Interdisciplinary Institute for Neuroscience, UMR 5297, F-33000 Bordeaux, France
[3]Bordeaux Imaging Center, UMS 3420 CNRS, US4 INSERM, University of Bordeaux, F-33000 Bordeaux, France
[4]Co-senior authors
*Correspondence: eric.hosy@u-bordeaux.fr (E.H.), daniel.choquet@u-bordeaux.fr (D.C.)
http://dx.doi.org/10.1016/j.neuron.2015.01.012

SUMMARY

Short-term plasticity of AMPAR currents during high-frequency stimulation depends not only on presynaptic transmitter release and postsynaptic AMPAR recovery from desensitization, but also on fast AMPAR diffusion. How AMPAR diffusion within the synapse regulates synaptic transmission on the millisecond scale remains mysterious. Using single-molecule tracking, we found that, upon glutamate binding, synaptic AMPAR diffuse faster. Using AMPAR stabilized in different conformational states by point mutations and pharmacology, we show that desensitized receptors bind less stargazin and are less stabilized at the synapse than receptors in opened or closed-resting states. AMPAR mobility-mediated regulation of short-term plasticity is abrogated when the glutamate-dependent loss in AMPAR-stargazin interaction is prevented. We propose that transition from the activated to the desensitized state leads to partial loss in AMPAR-stargazin interaction that increases AMPAR mobility and allows faster recovery from desensitization-mediated synaptic depression, without affecting the overall nano-organization of AMPAR in synapses.

INTRODUCTION

The alpha-amino-3-hydroxy-5-methyl-4-isoxazole-propionic acid (AMPA) subtype of glutamate receptors (AMPAR) mediates most of fast excitatory synaptic transmission in the mammalian central nervous system. AMPAR are formed of a core heterotetrameric structure composed of a combination of four subunits, GluA1–GluA4 (Traynelis et al., 2010), surrounded by a variety of auxiliary subunits (Schwenk et al., 2012). AMPAR are largely concentrated in the postsynaptic density (PSD), in front of presynaptic glutamate release sites, where they are stabilized through interactions between the various members of the AMPAR complex with a variety of intracellular and extracellular partners (Jackson and Nicoll, 2011; Shepherd and Huganir, 2007). AMPAR are not all stable in the synapse and around 50% move constantly by Brownian diffusion within the plasma membrane, promoting continuous exchanges between synaptic and extrasynaptic sites. This proportion is highly regulated by neuronal activity and other stimuli (Choquet and Triller, 2013).

The diffusion of AMPAR has long been considered to play a role only in controlling the accumulation of synaptic receptors in time scales ranging from seconds to minutes (Choquet and Triller, 2013; Shepherd and Huganir, 2007). In 2008, we proposed a new physiological role for AMPAR diffusion in the control of fast synaptic transmission over timescales of a few tens of milliseconds (Heine et al., 2008). We demonstrated, using paired-pulse stimulations in electrophysiological recordings and crosslinking of surface AMPAR with antibodies, that the rapid exchange of desensitized receptors by naive ones in the synapse is essential to maintain the fidelity of high-frequency synaptic transmission. In addition, AMPAR stabilization by PSD-95-potentiated frequency-dependent synaptic depression (Opazo et al., 2010). Conversely, accelerating AMPAR movements by removing the extracellular matrix (Frischknecht et al., 2009) accelerated recovery from paired-pulse depression. Altogether, we thus hypothesized that AMPAR diffusion allows synapses to sustain higher frequencies than the rate of AMPAR return from desensitization would normally allow (Choquet, 2010). Upon glutamate release, the postsynaptic area in which AMPAR can be opened does not exceed 100–200 nm in diameter due to their low apparent affinity for glutamate (Lisman et al., 2007). Within this small area, rapidly diffusing receptors can be renewed up to 30% within 10 ms considering a homogeneous distribution of AMPAR at the synapse (Heine et al., 2008). However, as more than 50% of receptors may be immobile in the synapse (Ashby et al., 2006; Heine et al., 2008), this raises questions about the mechanisms through which AMPAR diffusion could allow a fast enough exchange of receptors to allow a measurable impact on high frequency synaptic transmission.

The nanoscale spatial distribution of AMPAR in the synapse is highly heterogeneous (MacGillavry et al., 2013; Masugi-Tokita

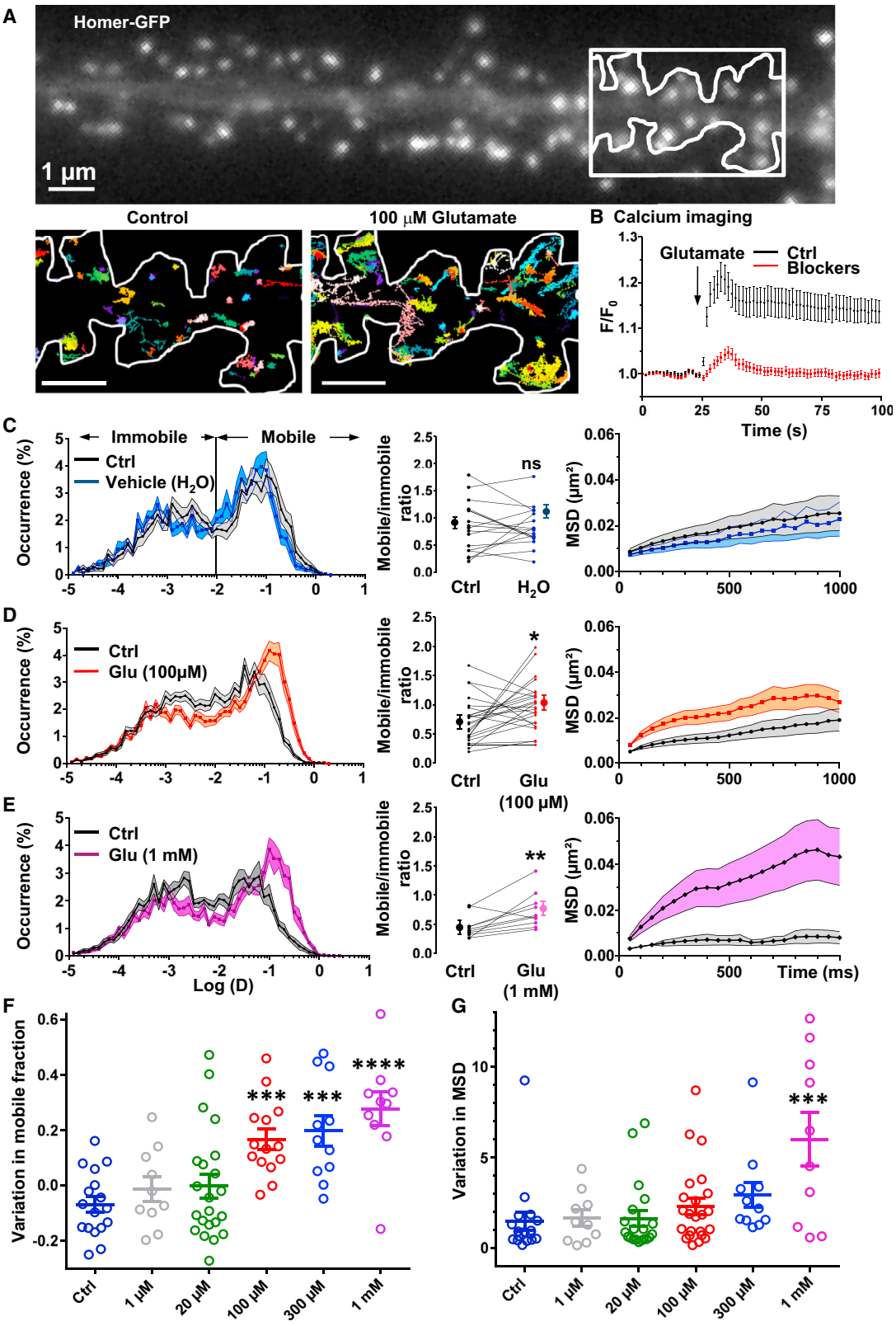

(legend on next page)

and Shigemoto, 2007; Nair et al., 2013). About half of synaptic AMPAR are packed and stabilized in clusters of about 80 nm wide, each comprising about 20 receptors. The other half are mobile in between clusters (Nair et al., 2013). While this could help explain how AMPAR diffusion could contribute to short-term plasticity, the relative stability of AMPAR nanodomains still poses the question of how a large proportion of trapped AMPAR could be exchanged within a few milliseconds.

Several molecular mechanisms are involved in controlling AMPAR stabilization, among which those mediated by the transmembrane AMPAR regulatory proteins (TARPs), and more particularly by stargazin, have been best characterized (Jackson and Nicoll, 2011). Stargazin is involved in stabilizing AMPAR in the PSD via its interaction with scaffolding proteins like PSD-95 (Bats et al., 2007; Opazo et al., 2010; Schnell et al., 2002) which is increased in long-term potentiation (LTP) via a CamKII-dependant phosphorylation of a stretch of serines in the stargazin C-tail (Opazo et al., 2010; Tomita et al., 2005b). Stargazin also modulates receptor pharmacology and controls channel gating: it increases AMPA receptor glutamate affinity, enhances single-channel conductance, slows deactivation and desensitization, and reduces the extent of desensitization (Priel et al., 2005; Tomita et al., 2005a; Turetsky et al., 2005).

The stability of stargazin (TARP)-AMPA receptor complex is controversial. Both the native and recombinantly expressed complexes have been reported to be readily disrupted by exposure to glutamate (Morimoto-Tomita et al., 2009; Tomita et al., 2004). The partial dissociation of the AMPAR/TARP complex within milliseconds after application of glutamate was further suggested using a tandem in which the amino-terminal part of stargazin is fused to the carboxy-tail of the receptor to prevent dissociation of the AMPAR/TARPs complex (Morimoto-Tomita et al., 2009). However, in other studies, rapid agonist-driven dissociation has not been observed (Nakagawa et al., 2005; Semenov et al., 2012).

Now, using single-particle tracking, biochemistry, and electrophysiology, we demonstrate that glutamate impacts AMPA receptor mobility through conformation changes: desensitized receptors being more mobile and less confined than those in the resting state due to specific unbinding of desensitized receptors from stargazin. This allows the desensitized fraction of receptors to move away from the glutamate release site and quickly be replaced by naive functional ones during synaptic transmission. Glutamate-mediated modulation of the mobility state of desensitized AMPAR directly participates to the modulation of frequency-dependent synaptic responses.

RESULTS

Glutamate Increases Mobility of Endogenous GluA2-Containing AMPAR

We first evaluated the impact of various doses of glutamate on the surface mobility of whole cell (see Figures S1A and S1B available online) and synaptic (Figure 1) endogenous GluA2-containing AMPAR in conditions of minimal intracellular signaling by using uPAINT single-molecule tracking of fluorescently labeled antibodies specific to the extracellular domain of GluA2 on dissociated hippocampal Banker cell cultures aged 13–16 days in vitro (DIV) (Giannone et al., 2010). On average, about 1,500 fluorescent AMPAR-bound antibodies were tracked each for at least 0.5 s (median value of trajectory duration in seconds with interquartile range [IQR],: 2.100 IQR 1.513–5.088), during recording periods of 3 min, both before and after application of glutamate (Figure 1A). In these conditions of short recordings, trajectory maps and partial superresolved pictures of the neurons before and after treatment can be reconstructed. Figure 1A represents a stretch of dendrite with synaptic areas identified by eGFP-Homer 1c expression, and shown below are AMPAR trajectories before and after application of 100 μM glutamate on an enlarged view of a dendrite segment. Glutamate application increased AMPAR mobility as evidenced by the larger area covered by AMPAR trajectories.

As previously described (Heine et al., 2008; Tardin et al., 2003), endogenous GluA2-containing AMPAR exhibit a variety of

Figure 1. Glutamate Increases Endogenous GluA2-Containing AMPAR Diffusion in Synapse

(A) Epifluorescence image of a dendritic segment expressing eGFP-Homer1c as a synaptic marker (top) and corresponding synaptic trajectories of endogenous GluA2-containing AMPAR before and after application of 100 μM glutamate (bottom) recorded in the boxed region on the top Homer image. Each trajectory map is obtained by overaccumulation of 2,000 images acquired with uPAINT technique.

(B) Effect of glutamate application on cytoplasmic calcium concentration. Normalized intensity of calcium-sensitive dye Fluo4FF-AM fluorescence is plotted versus time. Neurons preloaded with Fluo4FF-AM dye were imaged every 1.5 s for 2 min in Tyrode's solution (black curve, n = 16 cells) or in Tyrode's solution supplemented with various blockers (see Supplemental Experimental Procedures; red curve, n = 12 cells). After 25 s of recording, 100 μM glutamate was applied. In the absence of the inhibitor cocktail, glutamate triggered a large increase in the intracellular calcium level which was markedly decreased in the presence of the combination of blockers. Unless stated, error bars represent standard error of the mean (SEM).

(C) Absence of modulation of endogenous GluA2-containing AMPAR synaptic mobility upon addition of vehicle (water). GluA2-containing AMPAR were tracked using the uPAINT technique. Left panel shows the average distribution of the logarithm of the diffusion coefficient. Middle panel shows paired ratio of the mobile over the immobile fraction before and after treatment, and averages are represented on the sides (n = 17 cells, paired t test, $p > 0.05$). Right panel is the representation of the synaptic mean square displacement (MSD) as a function of time before and after treatment (n = 17 cells, t test on the under curve area, $p = 0.29$).

(D and E) Modulation of endogenous GluA2-containing AMPAR synaptic mobility by application of glutamate 100 μM (D) and 1 mM (E). From left to right are represented the average distribution of the logarithm of the diffusion coefficient, the paired ratios of the mobile over the immobile fraction (n = 24 cells, paired t test, $p = 0.023$ and n = 10 cells, paired t test, $p < 0.01$), and the plot of the synaptic MSD in function of time before and after treatment (n = 24 cells, t test on the under curve area, $p = 0.038$ and n = 10 cells, paired t test on the under curve area, $p < 0.001$).

(F) Dose-response curve for changes in the paired ratio of mobile over the immobile fraction following addition of varying glutamate concentrations (or vehicle for control). Five glutamate concentrations are tested from 1 μM to 1 mM. A significant increase of the AMPAR mobility is observed for concentrations $\geq$100 μM (mean ± SEM are plotted, statistical test is one-way ANOVA with Dunnet's post test).

(G) Dose-response curve for change in the area under the mean square displacement following addition of various glutamate concentrations (or vehicle control; mean ± SEM are plotted, statistical test is one-way ANOVA with Dunnet's post test).

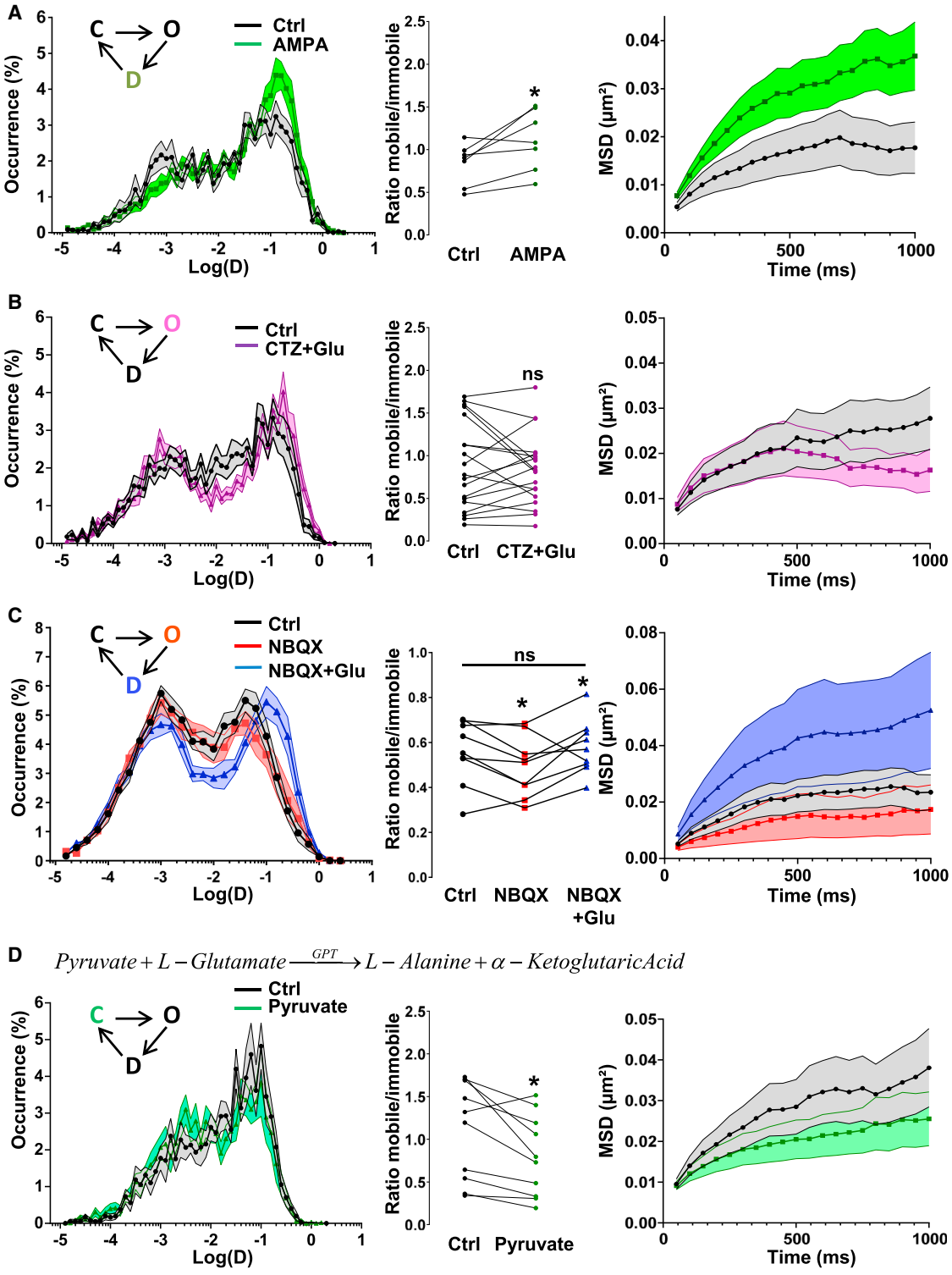

Figure 2. Drug Applications Reveal that Glutamate-Induced Mobility Is Specific of the Desensitized State

(A) Modulation of endogenous GluA2-containing AMPAR synaptic mobility in the presence of AMPA (100 µM) in drug-free Tyrode's solution. From left to right are represented the average distribution of the logarithm of the diffusion coefficient, the paired ratios of the mobile over the immobile fraction (n = 7 cells, paired t test, $p < 0.05$) and the plot of the synaptic MSD in function of time before and after treatment (n = 7 cells, paired t test on the under curve area, p = 0.01). AMPA increase significantly AMPAR mobility.

(legend continued on next page)

diffusion phenotypes ranking from immobile to highly mobile (Figure S1A). The diffusion coefficient (D) distribution can be roughly sorted into two groups. The first group is composed of AMPAR with a D value inferior to 0.008 $\mu m^2.s^{-1}$ and are referred to as "immobile" because they explore an area inferior to the one defined by the image spatial resolution (e.g., 0.08 μm) within one frame, i.e., 50 ms ($D_{threshold}$ = [0.08 μm]^2/[4 × 4 × 0.05 s] ~0.008 $\mu m^2.s^{-1}$). The second group is defined as the mobile part composed of receptors with D values above 0.008 $\mu m^2.s^{-1}$.

To investigate the effect of glutamate binding on AMPAR lateral mobility, independently of downstream intracellular signaling effects, we used acute application of various glutamate concentrations to the recording medium in the presence of a cocktail of inhibitors of (non-AMPA)-glutamate receptors and calcium channels while performing uPAINT acquisition. First, to estimate the effect of glutamate application on global cell signaling in these conditions, we measured the cytoplasmic calcium rise induced by glutamate. Neurons were preloaded with Fluo4FF-AM dye and then imaged every 1.5 s during 2 min in the observation medium. After 25 s of recording, 100 μM of glutamate was added. In the absence of the inhibitors, glutamate triggered a large increase in intracellular calcium level (Figure 1B, black line). The glutamate-induced calcium rise was markedly decreased in the presence of a combination of inhibitors of NMDA receptors, voltage-dependant Na^+ channels, L-type Ca^{2+} channels, mGluR1, mGluR5, and GluA2-subunit lacking AMPAR (Figure 1B). At the peak, in absence of blockers (Figure 1B, black line), the normalized fluorescence F/F_0 increased by 22.2% ± 3.7% compared to baseline level, whereas in presence of all blockers (Figure 1B, red line), this rise was limited to 2.2% ± 1.3%. We performed the recording in the presence of this inhibitors cocktail for all further experiments, unless otherwise stated.

Figures 1C–1G quantifies the effect of glutamate addition. In the presence of 100 μM glutamate, the proportion of mobile AMPAR increased by 30.7% ± 9.4% as compared to control, leading to an increase by 70.6% ± 22.4% of the ratio between the mobile and the immobile fractions of receptors (n = 24 cells, paired t test, p = 0.023) (Figure 1D). In parallel, the MSD, that represents the surface explored by the receptors per unit time, increased by ~70% in the presence of glutamate (Figure 1D, right panel). Application of a lower glutamate concentration (20 μM) or of the vehicle (water) did not induce a significant modification in the mobile/immobile ratio (Figures S1B and 1C and dose response curve, respectively). In contrast, the application of higher glutamate concentration (300 μM and 1 mM) increased the mobile fraction and decreased the confinement of the receptors (Figure 1E and dose response curve, Figures 1F and 1G). Altogether, these experiments suggest that glutamate modifies, in a dose-dependent manner, AMPAR mobility at the synaptic plasma membrane independently of downstream signaling, and possibly directly through changes in receptor conformation.

To confirm that the effect of glutamate on AMPAR mobility was mediated directly by their activation, we applied the AMPAR-specific agonist AMPA (alpha-amino-3-hydroxy-5-methylisoazol-4-propionate) and characterized its effect on diffusion in the absence of the antagonist cocktail present in the other experiments (Figure 2A). Application of AMPA 100 μM leads to a significant increase in GluA2 mobility (44.6% ± 3% for the control and 51.4% ± 3.2% in the presence of AMPA, p = 0.014 paired t test), and an increase of 204% of the initial confinement area.

Glutamate triggers two major changes in AMPAR conformation, first a transition to an open-state and then, within a couple of milliseconds, a transition to a desensitized state (Armstrong et al., 1998; Dürr et al., 2014; Meyerson et al., 2014; Sobolevsky et al., 2009; Sun et al., 2002). To correlate the glutamate-induced increase in AMPAR mobility to one or the other conformational state, we coapplied 100 μM glutamate with 20 μM cyclothiazide (CTZ), which prevents entry in the desensitized state; in this condition most receptors are in the open state (Traynelis et al., 2010) (Figure 2B). Neither the diffusion coefficient nor the MSD of synaptic AMPAR was affected by this treatment. This indicates that AMPAR desensitization, rather than opening, increases its mobility.

In our experiments, ambient glutamate released by neurons in culture could affect the mobility. To test this hypothesis, we first used an AMPAR antagonist (NBQX) to favor the closed-resting state. NBQX (20 μM) significantly decreased the mobile fraction and increased the confinement of AMPAR (Figure 2C). Supplementing 100 μM glutamate to the medium was presumably sufficient to compete out NBQX from enough binding sites to send AMPAR to a desensitized state, since we observed an increase in AMPAR mobility. To confirm the effect of ambient glutamate on AMPAR mobility, we recorded wild-type AMPAR mobility in

(B) Absence of modulation of endogenous GluA2-containing AMPAR synaptic mobility by coapplication of 100 μM glutamate and 20 μM cyclothiazide. From left to right are represented the average distribution of the logarithm of the diffusion coefficient, the paired ratios of the mobile over the immobile fraction (n = 19 cells, paired t test, p = 0.539), and the plot of the synaptic MSD in function of the time before and after treatment (n = 19 cells, paired t test on the under curve area, p = 0.28). Neither the diffusion coefficient nor the MSD of synaptic AMPAR are affected by coapplication of glutamate and cyclothiazide, which stabilized the AMPAR open state.

(C) Modulation of endogenous GluA2 containing AMPAR synaptic mobility by sequential application of NBQX (20 μM) (competitor antagonist), then additionally glutamate (100 μM). From left to right are represented the average distribution of the logarithm of the diffusion coefficient and the paired ratios of the mobile over the immobile fraction (n = 9 cells, p < 0.05). NBQX significantly immobilizes AMPAR by closing the ones desensitized by ambient glutamate, and then addition of extra glutamate reversed the effect on AMPAR mobility, suggesting that high glutamate concentrations are capable of competing with NBQX to send AMPAR into a desensitized state. Right panel is the plot of the synaptic MSD in function of time before and after treatment (n = 9 cells, repeated-measures ANOVA test on the under curve area, p < 0.05).

(D) Average distribution of the logarithm of the diffusion coefficient for synaptic endogenous GluA2-containing AMPAR before and after coapplication of glutamic-pyruvate transminase (GPT) and pyruvate to convert glutamate to L-alanine and α-ketoglutaric acid, thus decreasing the ambient glutamate. The middle panel is the mean ratio of the mobile over the immobile fractions of synaptic receptors before and after application of GPT and pyruvate (n = 10 cells, paired t test, p = 0.015). Scavenging ambient glutamate decreases synaptic AMPAR mobility. The right panel represents the synaptic MSD versus time plot before and after coapplication of GPT.

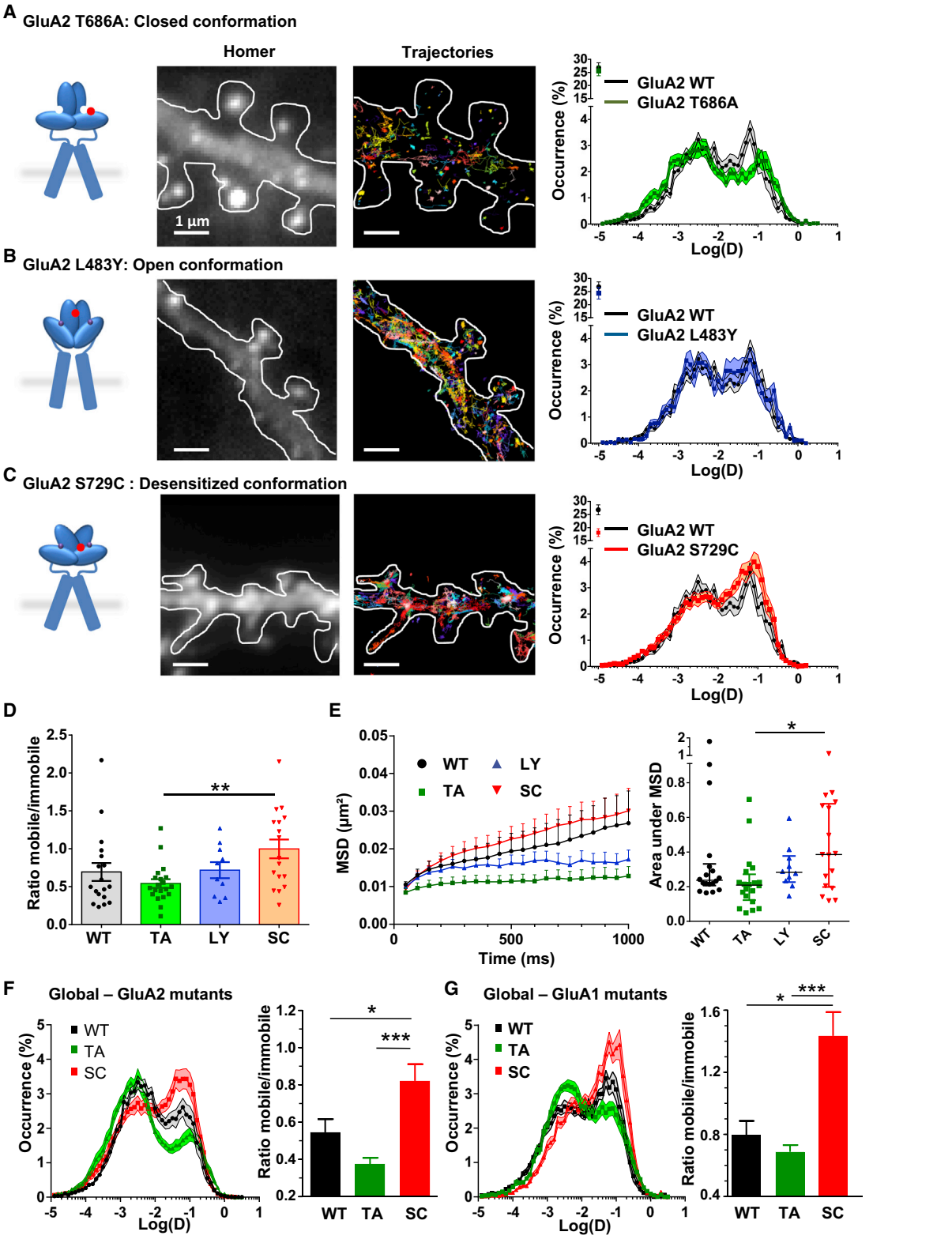

(legend on next page)

the presence of glutamic-pyruvic transaminase (GPT), an enzyme that degrades the ambient glutamate when pyruvate is in excess. Figure 2D shows that acute degradation of ambient glutamate triggers a significant decrease of AMPAR mobility. Finally, in conditions of ambient glutamate, evaluated to be in the micromolar range in hippocampal cultures (Featherstone and Shippy, 2008), a fraction of AMPAR are desensitized (Heine et al., 2008). Application of CTZ in this basal condition, which favors the AMPAR closed state, decreased the fraction of mobile receptors (Figure S1C). Altogether, these experiments demonstrate that basal ambient glutamate is sufficient to significantly increase AMPAR diffusion, likely by increasing the proportion of desensitized receptors, and further suggests that the closed AMPAR are the least mobile.

To analyze the specificity of the glutamate-induced increase mobility for AMPA-type glutamate receptors, we performed uPAINT experiments on kainate receptors (KARs) containing the GluK2 subunit which have similar conformational changes to AMPAR. We expressed Super Ecliptic pHluorin (SEP)-tagged GluK2 to track them with uPAINT using an anti-GFP nanobody. At rest, the diffusion coefficient of GluK2 was lower than that of GluA2 containing AMPAR (median values of the diffusion coefficient D in $\mu m^2.s^{-1}$ with IQR for synaptic GluK2 0.00067 IQR 0.00001–0.01655; for synaptic GluA2 0.00389 IQR 0.000225–0.03900). Application of 100 μM glutamate did not modify the diffusion coefficient nor the MSD over time of GluK2 (Figure S1D). This suggests that although they share common structural properties, the lateral diffusion of KARs and AMPAR is impacted differently by glutamate.

AMPAR Conformation Impacts Its Mobility

To examine if desensitized receptors are indeed more mobile than receptors in other states, we measured the mobility of various AMPAR mutants stabilized in distinct conformational states. We started by mutating the GluA2 subunit, as it is the one we tracked for our experiments on endogenous AMPAR. To measure the mobility of AMPAR largely occupying the closed-resting state, we used the T686A mutation in GluA2 (Robert et al., 2005). In contrast, the L483Y GluA2 mutant is stabilized in an open conformation (Stern-Bach et al., 1998; Sun et al., 2002). Finally, for receptors in a desensitized state, we used the S729C GluA2 mutant, which undergoes spontaneous disulfide bond formation that stabilizes a conformation associated with desensitization (Armstrong et al., 2006; Plested and Mayer, 2009). These mutated receptors were tagged with SEP and tracked with ATTO 647N labeled anti-GFP nanobodies (Figure S2).

As with endogenous AMPAR, exogenous wild-type GluA2 containing AMPAR displays a two-peak synaptic mobility distribution (Figure 3A, right panel, black curve). GluA2 T686A-containing AMPAR, which are mainly in a closed state, displayed a large increase in their immobile fraction correlated with a decrease in the mobile/immobile ratio of ~15% compared with recordings of overexpressed wild-type GluA2 containing AMPAR (Figure 3A right panel; Figure 3D, green curve and bar). Concomitantly, GluA2 T686A displayed an increase in their confinement compared to the nonmutated ones, as evidenced by their lower MSD (Figure 3E, green curve). In parallel, to confirm the insensitivity of GluA2 T686A-containing AMPAR to glutamate, we measured the effect of 100 μM glutamate application on GluA2 T686A mobility. Neither the mobility nor the confinement indexes of GluA2 T686A subunits are affected by glutamate (Figure S3A). This lower mobility and higher confinement of T686A AMPAR compared to wild-type ones (Figures 3D and 3E) is likely due to the partial desensitization of the latter by residual glutamate in the medium and to a couple of outlier cells displaying higher mobility (Figures 3D and 3E, WT).

In contrast to the T686A mutant, mobility of the GluA2 L483Y subunit, which stabilizes the open state in the presence of glutamate, presents similar diffusion properties and confinement values to the wild-type receptor (Figure 3B and Figures 3D and 3E, blue bar and curve). These results confirm the experiments performed when coapplying glutamate and cyclothiazide and

Figure 3. Mutated GluA2 Stabilized in a Desensitized State Are More Mobile than GluA2 Locked in a Closed or Open Conformation

(A–C) The left panels depict schemes representing the tracked AMPAR stabilized in specific conformations using point mutations. On each scheme, only the LBD, linkers, and TMD of a dimer of GluA2 are depicted. Red dots localize the point mutations. Image panels from left to right show the epifluorescence image of DsRed-Homer1c in a sample neuron, a map of the recorded trajectories using the uPAINT technique in the corresponding stretch of dendrite, and the total distribution of the logarithm of the synaptic diffusion coefficient. On each distribution, the dark line represents the control distribution of WT GluA2. (A) Comparison between GluA2 WT and T686A, a mutant stabilized in the closed state. (B) Comparison between GluA2 WT and L483Y, a mutant stabilized in the open state and so cannot desensitize. (C) Comparison between GluA2 WT and S729C, a mutant stabilized in a desensitized state. The mobile fraction of AMPAR is enriched when the receptor is stabilized in a desensitized conformation (red plot) relative to the ones in the closed/resting state (green and blue plots from A and B).

(D) Mean ratio of the mobile over the immobile fractions (±SEM) for synaptic overexpressed SEP-GluA2 and conformational mutants of GluA2 (WT, n = 17 cells; T686A, n = 20 cells; L483Y, n = 10 cells; S729C, n = 17 cells; one-way ANOVA, p = 0.0161, and Sidak's post test p = 0.009, between T686A and S729C). The ratio between the mobile and the immobile fraction is increased when the receptor stays in a desensitized conformation (red bar) compared to when it is in a closed/resting state (green bar).

(E) Plot of the synaptic MSD versus time for overexpressed SEP-GluA2 and the conformational mutants of GluA2 (left panel). Desensitized receptors (red plot) are less confined than closed/resting ones (green plot) (mean ± SEM, one-way ANOVA, p = 0.03, Sidak's post test show that TA/SC is significantly different p = 0.02). Median (±IQR) of the area under MSD are also represented (right panel) to illustrate cell to cell variability.

(F) Average distribution of the logarithm of the diffusion coefficient of pooled dendritic and synaptic overexpressed SEP-GluA2 and conformational mutants of GluA2. The right panel is the mean ratio of the mobile over the immobile fractions of pooled dendritic and synaptic overexpressed SEP-GluA2 and its conformational mutants (WT, n = 18 cells; T686A, n = 20 cells; S729C, n = 17 cells, one-way ANOVA test, and Sidak's post test).

(G) Average distribution of the logarithm of the diffusion coefficient of pooled dendritic and synaptic (left panel) overexpressed SEP GluA1 and its conformational mutants. Mean ratio of the mobile over the immobile fractions for overexpressed SEP GluA1 and its conformational mutants of GluA1 (WT, n = 9 cells; T686A, n = 14 cells; S729C, n = 11 cells; separate one-way ANOVA tests for mutants, with Dunnet's post test).

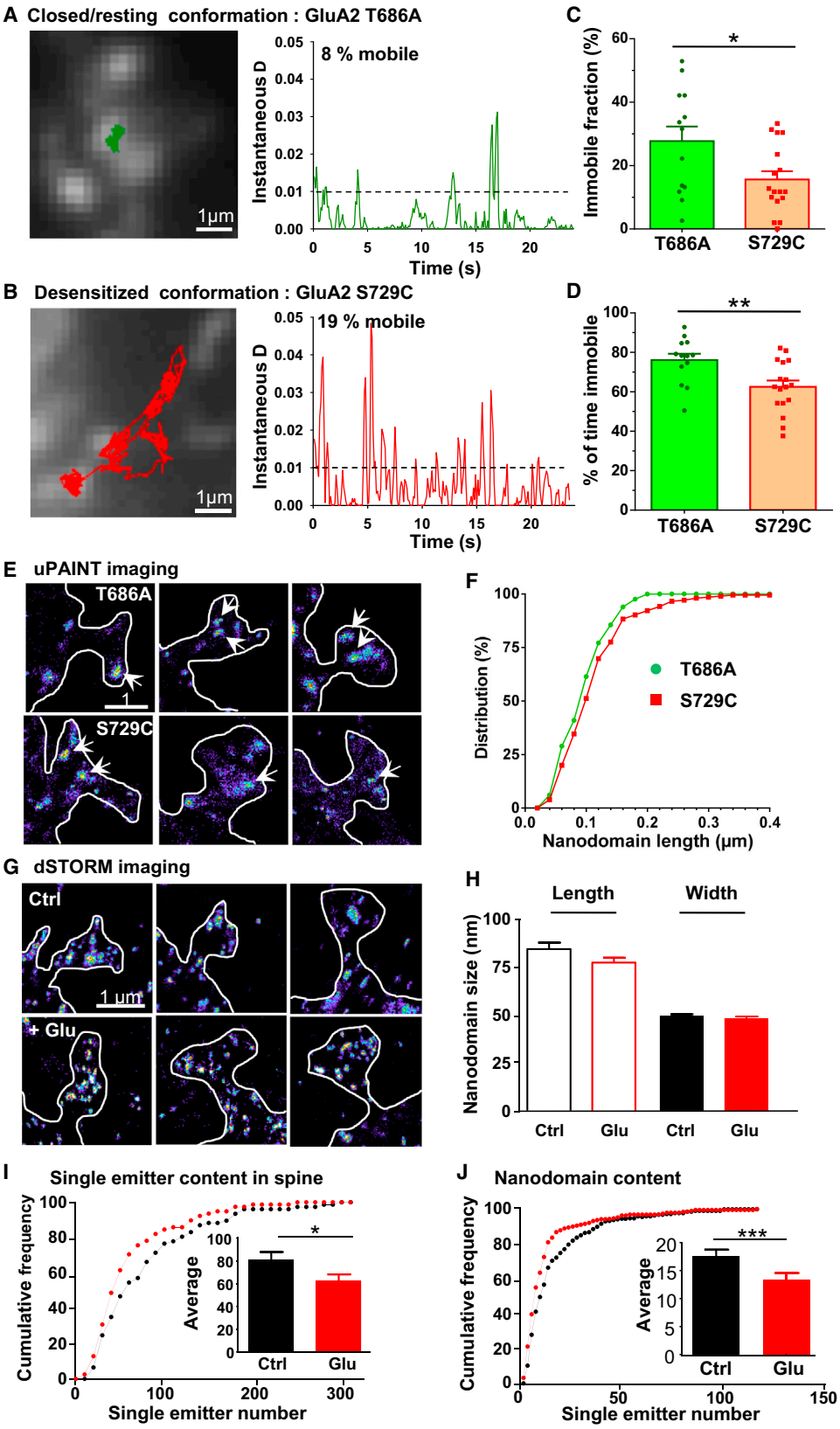

(legend on next page)

indicate the absence of a detectable change in mobility between closed and open receptors.

Finally, we expressed the GluA2 S729C mutant, which is stabilized in a desensitized state. We observed a striking 1.3-fold higher mobility of desensitized synaptic receptors as compared to those in a closed state (median values of the synaptic immobile fraction in % with IQR for GluA2 S729C 53.30 IQR 41.95–64.05; for GluA2 T686A 67.05 IQR 61.65–71.40; unpaired t test p = 0.0016). The mobile/immobile ratio of GluA2 S729C desensitized receptors is significantly higher to that of closed GluA2 T686A or wild-type receptors and similarly, the surface explored by GluA2 S729C is larger than the one explored by wild-type or always closed receptors (Figures 3C–3E). These effects were even more striking when measured on total surface GluA2 receptors (Figure 3F), as expected, since mobile receptors tend to escape from synaptic sites. The three corresponding point mutations in GluA1 induced similar and even more marked modifications in AMPAR mobility, indicating that the conformation dependent AMPAR mobility is largely subunit independent (Figures 3G and S3B).

Altogether, the increase in mobility of wild-type endogenous receptors induced by glutamate and AMPA and the increased mobility of mutants locked in a desensitized conformation indicate that desensitized AMPAR are more mobile than closed or open ones. This suggests that glutamate-induced conformation changes leading to the desensitized state may trigger release of receptors from synapses.

Desensitized AMPAR Are Stabilized for Shorter Durations than Closed-Resting AMPAR

We analyzed individual synaptic trajectories of T686A and S729C mutants lasting at least 2.5 s on neurons. For each time frame, an instantaneous diffusion coefficient was calculated (Figures 4A and 4B). This gives access to the evolution of the mobility of each receptor in function of time, allowing the extraction of two parameters: the percentage of totally immobile trajectories (log(D) < −2.1; Figure 4C) and the fraction of time spent immobile (Figure 4D). The fraction of immobile receptors all along their trajectory is significantly smaller for desensitized than for closed receptors (Figure 4B, unpaired t test, p = 0.023). In parallel, for receptors that alternate between mobile and immobile states, the proportion of time spent immobile is lower for desensitized receptors than for closed ones (Figure 4C, unpaired t test, p = 0.007). Similarly, glutamate significantly decreased the retention time of endogenous synaptic receptors (decrease of 10.5% ± 4.6%, n = 17, paired t test, p = 0.015). Altogether, this indicates that desensitized receptors are trapped less efficiently at synapses, resulting in a diminution in the proportion of immobile receptor in the spine and a corresponding higher exchange rate.

Glutamate-Mediated Increase in AMPAR Mobility Is Not Correlated with a Change in their Nano-organization

We next investigated whether AMPAR nanoscale organization depends on their conformational state. We and others previously demonstrated that wild-type and expressed AMPAR are organized in nanodomains with a full width at half maximum of ~70 nm (MacGillavry et al., 2013; Nair et al., 2013). The T686A and S729C GluA2 mutants formed nanodomains of similar size, as measured by anisotropic Gaussian fitting of presegmented clusters obtained on uPAINT high-resolution intensity images (Nair et al., 2013) (Figures 4E and 4F). This indicates that although desensitized AMPAR spend proportionally less time in the immobile state, their overall nanoscale organization is similar to that of closed receptors.

To confirm this finding, we performed d-STORM experiments on endogenous GluA2 subunits before and after application of glutamate (Figure 4G). The nanodomain size did not vary significantly upon glutamate application (median values of the length (l) and width (w) in nm with IQR in control condition: w = 46.9 IQR 39.9–58.1; l = 75.4 IQR 55.65–104.5 and after glutamate treatment: w = 46.4 IQR 39.19–56.64; l = 67.95 IQR 56.0–88.58; Mann-Whitney test, p = 0.6203 for width, p = 0.1856 for length; Figure 4H). In parallel, we estimated the total number of

Figure 4. Glutamate-Induced Increase in Mobility Is Due to a Remobilization of Trapped Receptors without Affecting Nanodomain Structure

(A and B) Representative synaptic trajectories and the variation of their instantaneous diffusion versus time obtained by tracking GluA2 S729C and GluA2 T686A conformational mutants, respectively. The dark dashed line represents the threshold under which receptors are considered as immobile. S729C mutant are more mobile than the T686A ones. Two parameters can be extracted from these trajectories. The first one is the fraction of receptors which are immobile (C). The second one is the fraction of time AMPAR are immobile measured on trajectories which alternate between mobile and immobile behavior (D).

(C) Fractions of receptors which are immobile (log [D] < −2.1) all along their trajectory duration for GluA2 S729C and GluA2 T686A mutants (mean ± SEM; n = 17 cells for GluA2 S729C, n = 13 cells for GluA2 T686A, unpaired t test, p = 0.023).

(D) Percentage of time AMPAR are immobile on their trajectory when they are partially mobile for GluA2 S729C and GluA2 T686A (mean ± SEM; n = 17 cells for GluA2 S729C, n = 13 cells for GluA2 T686A, unpaired t test, p = 0.007).

(E) Sample superresolved intensity images obtained by uPAINT on neurons expressing GluA2 T686A (top) or GluA2 S729C (bottom). Arrows point to AMPAR nanodomains. Distribution of AMPAR nanodomain length measured for GluA2 S729C and GluA2 T686A (F). Nanodomain sizes are similar for receptors locked in the desensitized or in the closed conformation (S729C, n = 205 nanodomains; T686A, n = 83 nanodomains; Mann-Whitney test, p = 0.086).

(G) Sample superresolution intensity images of spines obtained using d-STORM on neurons live stained for endogenous GluA2. After live incubation with antibodies against GluA2, neurons were incubated for 2 min either in the presence of vehicle (top) or in the presence of 100 μM glutamate (bottom).

(H) Width and length of AMPAR synaptic nanodomains. Nanodomain sizes were measured by anisotropic Gaussian fitting clusters obtained on d-STORM images. Nanodomain length and width (mean ± SEM) in control conditions and after application of 100 μM glutamate are plotted (left, n[ctrl] = 149 and n[Glu] = 174 nanodomains, Mann-Whitney test, p > 0.1 for both width and length). Nanodomain size is not impacted by glutamate application.

(I and J) Cumulative distribution and, in the insert, mean of spine and nanodomain AMPAR content, respectively. The total number of AMPAR inside spines was estimated by counting the single emitters. The cumulative distribution and the average number of single emitters per spines are reported in control and glutamate treated conditions (mean ± SEM; n = 77 and 78 spines, respectively; Mann-Whitney test, p = 0.038). As for the spine level, the number of AMPAR in nanodomains was estimated in control and glutamate treated conditions (mean ± SEM; n = 226 and 189 nanodomains, respectively, Mann-Whitney test, p < 0.0001). Upon glutamate treatment, the number of AMPAR inside both spines and nanodomains significantly decreases.

AMPAR present in spines and in individual nanodomains before and after glutamate treatment by dividing the total number of single-molecule detection events in a spine or a nanodomain by the average number of detection events determined for isolated fluorescent spots that likely represent individual receptors (Nair et al., 2013). Cumulative frequencies of the number of single emitters per spine and nanodomain are represented in Figures 4I and 4J. In both cases, we observed a decrease of ~20% in the number of single emitters when neurons were treated with glutamate (median values of the number of single emitters per spine [s] and per nanodomain [n] with IQR in control condition: s = 58.13 IQR 34.86–102.5, n = 11.02 IQR 6.673–22.01 and after glutamate treatment, s = 46.21 IQR 31.17–75.20, n = 8.337 IQR 5.481–13.40). This represents a loss of ~12 AMPAR per spine (Figure 4I) and three AMPAR per nanodomain upon glutamate application (Figure 4J). Altogether these data indicate that glutamate mediates a mobilization of synaptic AMPAR which leads to a loss of receptors contained in spines and nanodomains. This is not associated with a major change in their subsynaptic organization at the nanoscale level.

Molecular Basis of Glutamate-Induced Increase in AMPAR Mobility

We and others previously demonstrated (Bats et al., 2007; Nair et al., 2013; Opazo et al., 2010; Schnell et al., 2002; Sumioka et al., 2010; Tomita et al., 2005a) that synaptic AMPAR stabilization is mainly based on interactions within a tripartite complex composed of the cytoplasmic scaffold PSD-95, the AMPAR auxiliary protein stargazin, and the AMPAR. To decipher the molecular basis of glutamate-induced increase in AMPAR mobility, we investigated possible modifications in the interaction between stargazin and AMPAR.

Previous work indicated that glutamate induces a dissociation of stargazin from AMPAR (Morimoto-Tomita et al., 2009; Tomita et al., 2004), although this has been debated (Nakagawa et al., 2005; Semenov et al., 2012). We thus investigated whether the glutamate-induced increase in AMPAR mobility could originate from a loss of avidity of stargazin for specific AMPAR conformational states. We coexpressed the various GluA1 mutants locked in the closed and desensitized conformation in HEK cells together with WT GluA2 and stargazin and used coimmunoprecipitation to measure their interaction (Figures 5A and 5B). Strikingly, the S729C desensitized mutant displayed a 60% reduction in binding to stargazin compared to WT and closed forms of GluA1. In order to further test if glutamate-induced stargazin detachment from AMPAR is at the origin of their increased mobility, we measured the effect of glutamate on the mobility of GluA1-stargazin tandems in which the intracellular C terminus of GluA1 is fused to the N terminus of stargazin (Figure 5D), preventing any possible dissociation. This tandem has been previously shown to form functional AMPAR (Morimoto-Tomita et al., 2009). The tandem was tracked by uPAINT using an ATTO 647N tagged anti-GFP nanobody. The tandem presented a decreased mobility compared to WT (compare Figures 5C and 5D), fully compatible with the key role of stargazin in immobilizing AMPAR (Bats et al., 2007). This stabilization was likely mediated through interactions with PSD scaffold proteins, since truncating the PDZ ligand of the chimeric GluA1-stargazin resulted in a construct with very high mobility (data not shown). Bath application of 100 μM glutamate did not increase the mobility nor the mobile/immobile ratio of the GluA1-stargazin tandem, while it increased both when GluA1 was expressed alone (Figures 5C and 5D). Moreover, after application of glutamate, the area explored by the tandem remained unchanged, whereas this area increased for GluA1 (Figures 5C and 5D, right panels). These experiments suggest that the glutamate-induced increase in AMPAR mobility is due to a decreased association of the AMPAR desensitized state with auxiliary proteins.

Acute Stimulation of Synapses by Glutamate Uncaging Mobilizes AMPAR

An important question is to know if the glutamate-induced increase in AMPAR mobility occurs physiologically since AMPAR desensitize even after a brief exposure to glutamate (Colquhoun et al., 1992). As a first step, we refined spatiotemporally the application of glutamate by using two-photon MNI-glutamate uncaging in the presence of the blockers used for bath application of glutamate (Figure 6A). We first verified that 2P glutamate uncaging triggers currents comparable to spontaneous excitatory postsynaptic currents (EPSCs) (Figure 6B). We then compared the mobility of AMPAR before and after uncaging, either at uncaged (Figure 6C) or neighboring synapses (Figure 6D) on the same neuron. Glutamate uncaging induced a specific increase in AMPAR mobility at uncaged synapses, supported both by an increase in the median diffusion and a decrease in the confinement. This increased mobility is more modest that the one observed during bath application of glutamate. This result was expected, since the area over which 2P uncaging is performed is small and the time of glutamate presence very short, while tracking measurements are performed during 0.5 s, a period during which a significant fraction of AMPAR have recovered from desensitization. We performed similar experiments with one-photon uncaging of MNI-glutamate and found similar results (Figure S4). Together, these results corroborate and refine our initial findings with bath application of glutamate: brief application of glutamate increases AMPA receptor mobility at synapses.

Glutamate-Induced Increase in Desensitized AMPAR Mobility Tunes Short-Term Synaptic Plasticity

We have previously shown that AMPAR fast diffusion tunes frequency-dependent synaptic transmission in paired-pulse experiments by allowing desensitized receptors to be replaced by naive ones, thus accelerating recovery from desensitization-induced synaptic depression (Frischknecht et al., 2009; Heine et al., 2008; Opazo et al., 2010). We thus investigated whether the glutamate-induced mobility of desensitized receptors could directly participate in explaining our previous findings that mobile AMPAR are necessary for fast recovery from synaptic depression during high frequency stimulus trains. To this aim, we performed whole-cell patch-clamp measurements of short-term synaptic plasticity in hippocampal neurons expressing SEP-GluA1 either alone or coexpressed with the tandem SEP-GluA1-stargazin. To investigate the impact of mobility, we used the classical antibody-mediated crosslink approach to immobilize expressed receptors and then applied 20 Hz stimulus

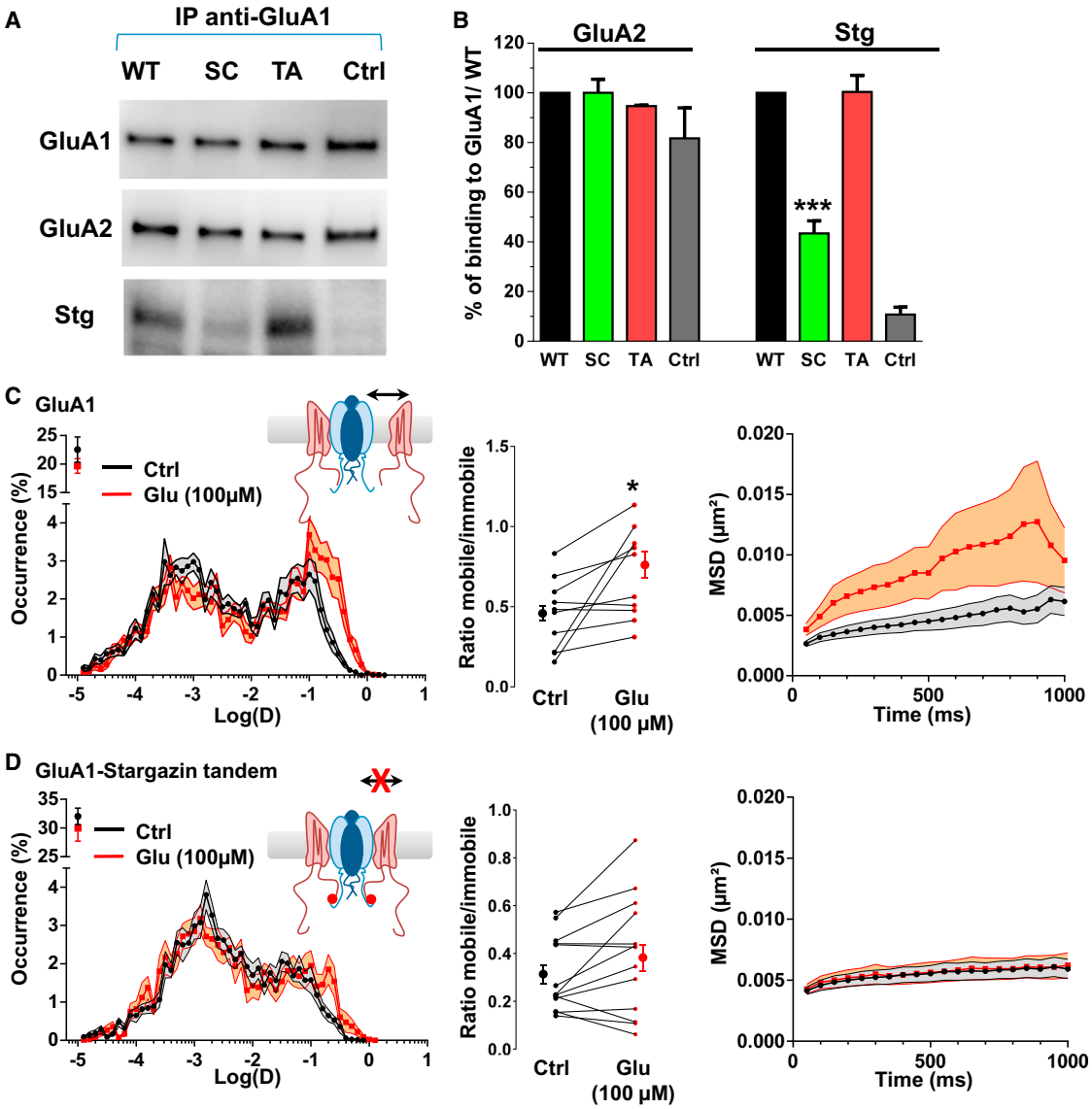

Figure 5. Glutamate-Induced AMPAR Mobility Is Abolished for the Chimera GluA1/Stargazin

(A) Coimmunoprecipitation experiment on extracts from HEK cells coexpressing GluA2 and wild-type, desensitized, or closed mutants of GluA1 with or without (Ctrl) stargazin as indicated in the figure. Immunoprecipitation of GluA1 was performed using an antibody directed against the extracellular domain. The samples were analyzed with anti-GluA1, anti-GluA2, and anti-Stg for each condition.

(B) Quantification of five GluA1/GluA2/stg immunoprecipitation experiments. The Stg binding to desensitized receptor is significantly reduced (mean ± SEM; n = 5 experiments, one-way ANOVA with Dunnet's post test).

(C and D) Left panel insets show schemes representing the hypothetical stargazin and GluA1 interactions and their corresponding mobility before and after glutamate application, in control condition (endogenous stargazin and expressed SEP-GluA1) in (C) and when the two proteins are genetically fused (SEP-GluA1-stargazin chimera) in (D). (Left panels) Distributions of the logarithm of the diffusion coefficients. Middle panels: paired ratio of the mobile over the immobile fraction before and after treatment with 100 μM glutamate (for GluA1: n = 10 cells, paired t test, p = 0.024; for GluA1-stargazin chimera: n = 13 cells, paired t test, p > 0.05). Glutamate mobilizes synaptic GluA1-containing AMPAR but not GluA1-stargazin chimera. Right panels show plots of the synaptic MSD versus time before and after application of glutamate (100 μM).

trains to stimulate presynaptic axons and evoke a series of EPSCs.

In control cells expressing SEP-GluA1, we observed short-term facilitation of the EPSCs. The fifth response was on average increased to 120% of the amplitude of the first EPSC of the train (Figures 7A and S5A). Consistent with what we demonstrated previously for paired-pulse protocols (Heine et al., 2008), cross-linking surface SEP-GluA1-containing AMPAR with an anti-GFP antibody for 5 min caused a marked decrease in the EPSC amplitudes during the train (p = 0.0301, Welch's two-tailed t test), where the fifth EPSC decreased to 78% of the amplitude for the first response of the train (Figure 7A). This short-term

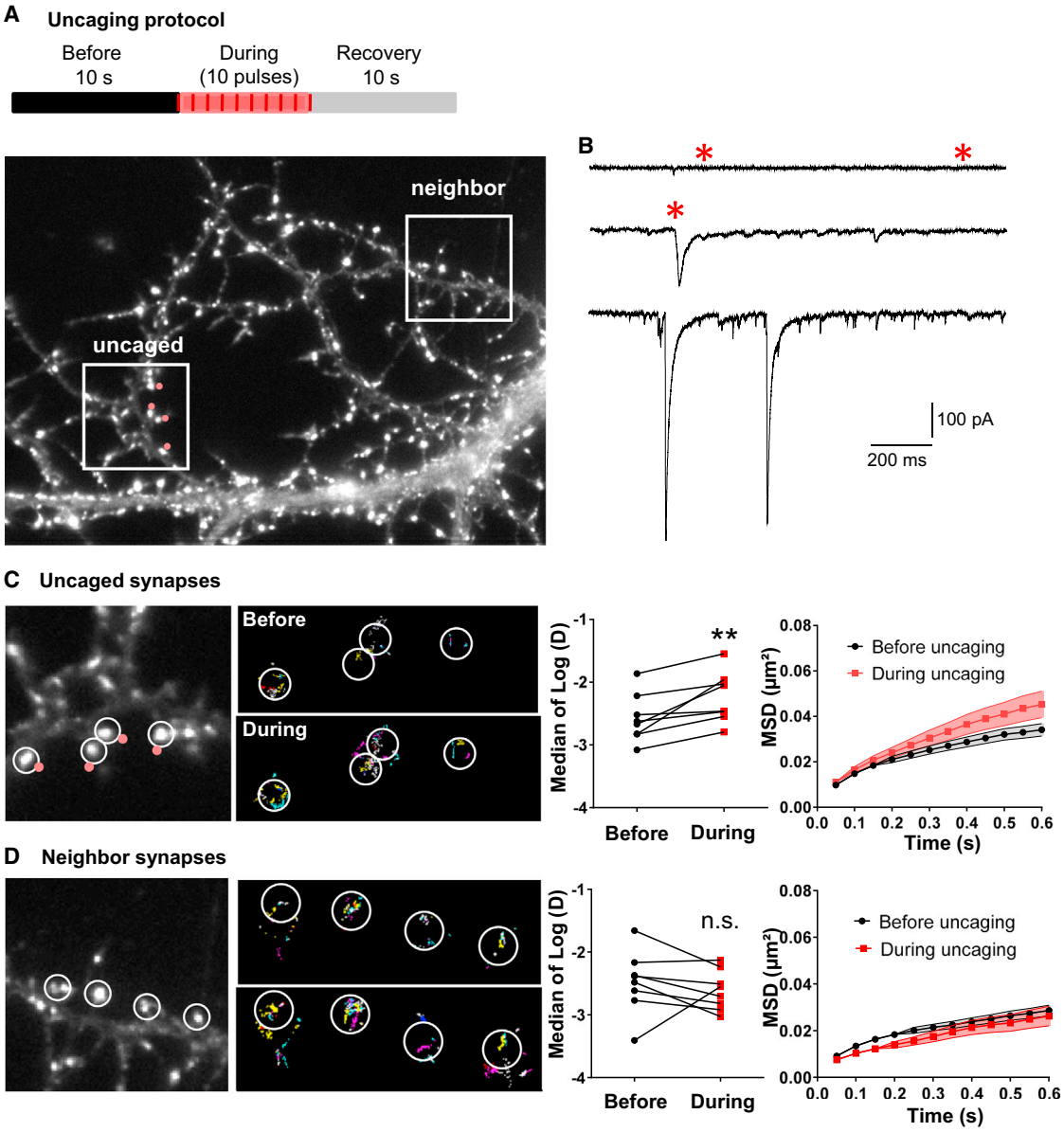

Figure 6. Acute Stimulation of Synaptic AMPAR with Glutamate 2-P Uncaging Mobilizes AMPAR

(A) Top panel shows an illustration of the protocol used for control and glutamate uncaging assays. Lower panel shows an epifluorescence image of a neuron expressing eGFP-Homer 1c as a synaptic marker and the position of uncaging spots indicated with red dots. One protocol round consists of a 10 s baseline recording followed by 10 uncaging laser pulses at 2 Hz, and by 10 s without recording and stimulation to avoid overstimulation. For each cell, five consecutive rounds were recorded.

(B) Examples of electrophysiological currents recorded in the presence of 2.5 mM MNI-glutamate when, from the top to the bottom, the laser is off (no uncaging), laser is on (uncaging) and when synaptic transmission occurred spontaneously and independently of the laser trigger.

(C and D) Left panels show epifluorescence images and synaptic GluA2 trajectories before and during laser pulses at the uncaged synapses (C) and the neighbor synapses (D). Middle and right panels show, respectively, the plots of the median mobility value per cell and the synaptic MSD versus time, before and during laser pulses. AMPAR are less confined after glutamate uncaging (n = 8 cells, paired t test $p < 0.01$ and $p > 0.05$ for uncaged and neighbor synapses, respectively).

depression did not appear to be associated with much larger initial EPSC amplitudes that could otherwise be expected for a higher release probability (Figure 7A). Corroborating the specificity of the antibody crosslink for expressed receptors, a depressive effect on short-term plasticity was not observed when applying the anti-GFP to cells expressing GluA1 without the amino-terminal SEP fusion (Figure S5A). We then performed similar experiments on neurons expressing the GluA1-stargazin tandem. In the control cells (without antibody crosslinking), the ESPCs already depressed during the train (fifth EPSC to 75%),

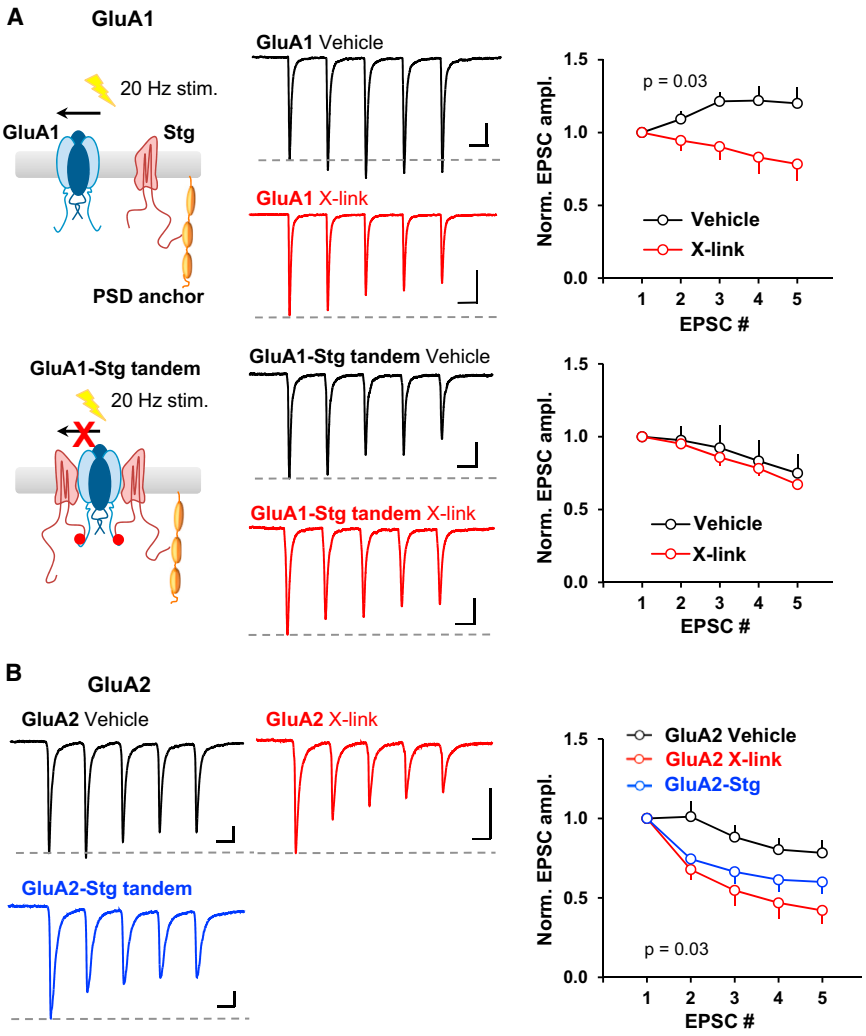

Figure 7. Train Stimulation Triggers Depression in Neurons Expressing the GluA-Stargazin Tandems, which Mimics and Occludes the Effect of AMPAR Crosslinking

(A) The diagrams on the left represent the experimental paradigm: SEP-GluA1 and endogenous stargazin are expressed separately or linked in a SEP-GluA1-stargazin tandem. GluA1 interact with stargazin (maroon, either endogenous or covalently linked) that traps AMPARs at synapses via PDZ interactions. To test the role of AMPAR mobility during a train of stimulation, lateral diffusion was blocked by crosslinking the receptors with an anti-GFP antibody (X-Link). The middle panels represent the average EPSC trains (five pulses at 20 Hz), for example cells in conditions with and without crosslinking. (Right) Plots of the EPSC amplitude normalized to the initial EPSC for stimulations with (n = 5 cells) and without (n = 6 cells) crosslinking. When GluA1 cannot dissociate from stargazin, EPSCs elicited by a train of stimulation already have depressed short-term plasticity, which occludes crosslinking (n = 7 cells, both with and without crosslinking).

(B) The same experiments performed with SEP-GluA2 and SEP-GluA2-Stg tandem (both coexpressed with SEP-GluA1) lead to a similar conclusion. (Left) Average EPSC trains for all cells in each group. (Right) Plots of EPSC amplitude with normalization to the initial EPSC. n = 15, 5, and 8 cells in the vehicle, X-link, and tandem conditions, respectively. (A and B) statistics with Welch's ANOVA test comparing the sum of normalized EPSC amplitudes. Log-transformed initial EPSC amplitudes were not significantly different in (A), top (p = 0.748, Welch's t test), or (B) (p = 0.260, Welch's ANOVA test). Scale bars are 50 pA and 25 ms.

likely as a direct consequence of the lower mobility of this construct (Figures 5D and 7A). We observed a similar effect on short-term plasticity when we coexpressed GluA1 with a GluA2-stargazin tandem (Figure 7B), indicating that the effect was not unique to the GluA1-stargazin tandem. Interestingly, when we tried crosslinking the GluA1-stargazin tandem, we did not observe much further depression during the train (fifth EPSC to 67%), thus demonstrating that fusion of GluA1 to stargazin occludes the depressive effect of crosslinking on short-term synaptic plasticity. Altogether, these experiments establish that preventing GluA1 or GluA2 dissociation from stargazin prevents the positive impact of AMPAR diffusion on recovery from short-term depression.

DISCUSSION

Using high-density single-molecule tracking on live and fixed neurons as well as biochemistry, electrophysiology, and glutamate uncaging, we investigated the impact of changes in AMPAR conformational states on their surface diffusion, confinement, and nanoscale organization. Our results on both wild-type AMPAR and point mutants of GluA1 and GluA2 subunits locked in various conformational states establish that desensitized AMPAR are more mobile than closed or open ones due to less avidity for stargazin. This glutamate-induced increase in AMPAR mobility removes a fraction (~20%–30%) of receptors from nanodomains and synaptic sites but does not modify the overall nanodomain organization of AMPAR. Finally, we show that the increased mobility of desensitized receptors plays a key role in fast synaptic transmission, enabling rapid turnover of AMPAR opposed to glutamate release sites. This allows synapses to recover faster from high-frequency short-term depression consequent to AMPAR desensitization.

Glutamate Binding Induces an Increase in the Proportion of Mobile AMPAR Independent of Intracellular Signaling

The use of single-molecule detection allowed us to obtain the full distribution of AMPAR behavior and detect that ~20%–30% of AMPAR increase their mobility upon glutamate binding in a dose-dependent manner. Glutamate has long been shown to regulate AMPAR traffic. Three main pathways have been

identified in this process. First, glutamate-induced increase in intracellular calcium during high-frequency stimulation triggers AMPAR immobilization and accumulation at synaptic sites (Borgdorff and Choquet, 2002; Heine et al., 2008; Opazo et al., 2010). This effect is largely mediated by CaMKII-induced phosphorylation of the AMPAR auxiliary protein stargazin, which stabilizes AMPAR by increasing binding to PSD-95. Second, the low-frequency stimulation induced increase in AMPAR mobility, which results in AMPAR loss from synaptic sites (Shepherd and Huganir, 2007; Tardin et al., 2003). Both these effects rely on intracellular signaling and have been proposed to underlie long-term synaptic plasticity. Third, and less characterized, activation of AMPAR has been proposed to trigger their endocytosis by a signaling-independent process (Beattie et al., 2000; Lin et al., 2000; Tomita et al., 2004). This is fully consistent with our observation that glutamate and AMPA induce an increase in AMPAR diffusion that does not depend upon intracellular signaling.

AMPAR Conformational Changes Trigger Their Increased Mobility

Glutamate binding triggers major changes in AMPAR conformation that lead to opening of the ion pore and ultimately entry into the desensitized state. Recent work on GluA subunits (Dürr et al., 2014; Meyerson et al., 2014; Nakagawa et al., 2005) indicates that, in the desensitized state, all the extracellular N-terminal domain composed by both the amino-terminal (ATD) and the ligand binding (LBD) domains undergo major rearrangements, resulting in a separation of the four subunits from 25 Å up to complete separation of the ATDs. Our experiments indicate that the AMPAR conformational changes triggered by glutamate are enough to increase their surface diffusion. First, bath glutamate application, glutamate uncaging, and even endogenous ambient glutamate trigger increased AMPAR diffusion. Second, pharmacological manipulations that favor either the AMPAR closed state (NBQX, Figure 2C) or prevent desensitization (CTZ, Figure S1C) slow down AMPAR. Third, point mutants of GluA1 or GluA2 that lock AMPAR in a desensitized conformation display a robust increase in diffusion as compared to wild-type AMPAR, or AMPAR locked in the closed or open conformations. Fourth, coapplication of glutamate and CTZ or expressing the LY mutation suggest that AMPAR in the open state move similarly to the closed ones. We have no certitude as to why the effect is more robust in GluA1 than GluA2 mutants, but this could simply arise from the more physiological expression of GluA1 than GluA2 homomers. In complement, we found that AMPA has a less profound effect on mobility than the physiological agonist, glutamate. Indeed, AMPA is known to trigger not exactly the same conformation changes in AMPAR as glutamate (Jin et al., 2003). Finally, recent results at the *Drosophila* neuromuscular junction also indicate that mutations changing gating properties alter GluR distribution and trafficking, although on a much slower timescale (Petzoldt et al., 2014).

Altogether, these studies and our results indicate that glutamate-induced entry of AMPAR into the desensitized state is associated with major structural rearrangements paralleled by increased receptor surface diffusion. Thus a major question is this: how could changes in the AMPAR ATD and LBD domains lead to their freeing from synaptic anchors?

Molecular Mechanism of Glutamate-Induced AMPAR Diffusion

Among all the protein-protein interactions accounting for AMPAR stabilization in the PSD, only a few are good candidates to be modulated by glutamate-induced AMPAR conformational changes. The GluA C terminus being largely nonstructured, it is hard to conceive how a change in the ATD/LBD organization could transfer into changes in GluA C terminus-scaffold interactions. Alternatively, the TARP family of AMPAR auxiliary subunits plays a central role in regulating AMPAR anchoring at synapses (Bats et al., 2007; Schnell et al., 2002). Stargazin binds AMPAR tightly through a large interface including the AMPAR extracellular domains (Cais et al., 2014; Tomita et al., 2004) and stabilizes the complex in the synapse through binding of its C terminus to PDZ domain-containing scaffolds such as PSD-95. The AMPAR-TARP-PSD-95 complex has been suggested to account in large part for basal and activity-dependent AMPAR immobilization at synapses (Bats et al., 2007; Opazo et al., 2010; Schnell et al., 2002; Tomita et al., 2005b). However, it is hard to conceive how a change in AMPAR conformation could translate into a decrease in TARP/PSD-95 interaction.

An initial biochemical study suggested that AMPAR dissociate rapidly from TARPs upon binding to glutamate and are internalized, whereas TARPs remain stable at the plasma membrane (Tomita et al., 2004), but in other following studies, rapid agonist-driven dissociation has not been observed (Nakagawa et al., 2005; Semenov et al., 2012). Most interestingly, we found now that the TARP-AMPAR interaction depends on AMPAR conformational state, desensitized AMPAR binding less stargazin. Our results thus indicate that increased AMPAR mobility upon glutamate binding is due to the specific dissociation of desensitized AMPAR from stargazin, allowing them to diffuse out of TARP anchoring sites at synapses such as PSD-95 slots (Figure 8). This dissociation could arise from the large structural rearrangement of the extracellular domain occurring upon AMPAR desensitization that likely impacts the normal engagement of both the ATD and LBD of AMPAR in the TARP-AMPAR interface (Cais et al., 2014). This hypothesis is supported by the fact that the GluA-stargazin tandems, which cannot be dissociated by glutamate binding, are less mobile than GluAs alone, and more importantly, that their mobility is not affected by glutamate.

While over 95% of AMPAR become desensitized within a few milliseconds upon glutamate binding (Colquhoun et al., 1992), we observed a change in mobility in only 35% of the receptors at the most. The large interface involved in AMPAR/TARP interaction (Cais et al., 2014; Priel et al., 2005; Tomita et al., 2005a; Turetsky et al., 2005) goes together with the high stability of the resting AMPAR/TARP complex reported in biochemical experiments (Schwenk et al., 2012; Tomita et al., 2004). We suggest that only some desensitized AMPAR have a lower affinity for TARPs, which is compatible with the existence of various desensitized AMPAR conformations (Dürr et al., 2014; Meyerson et al., 2014; Nakagawa et al., 2005). These various conformations would present different levels of mobility, depending on whether they are bound or not to a TARP. This hypothesis is further supported by our biochemical experiments that indicate a lower, but not fully abolished, binding of desensitized AMPAR to stargazin (Figure 5A). In addition, given the high density of

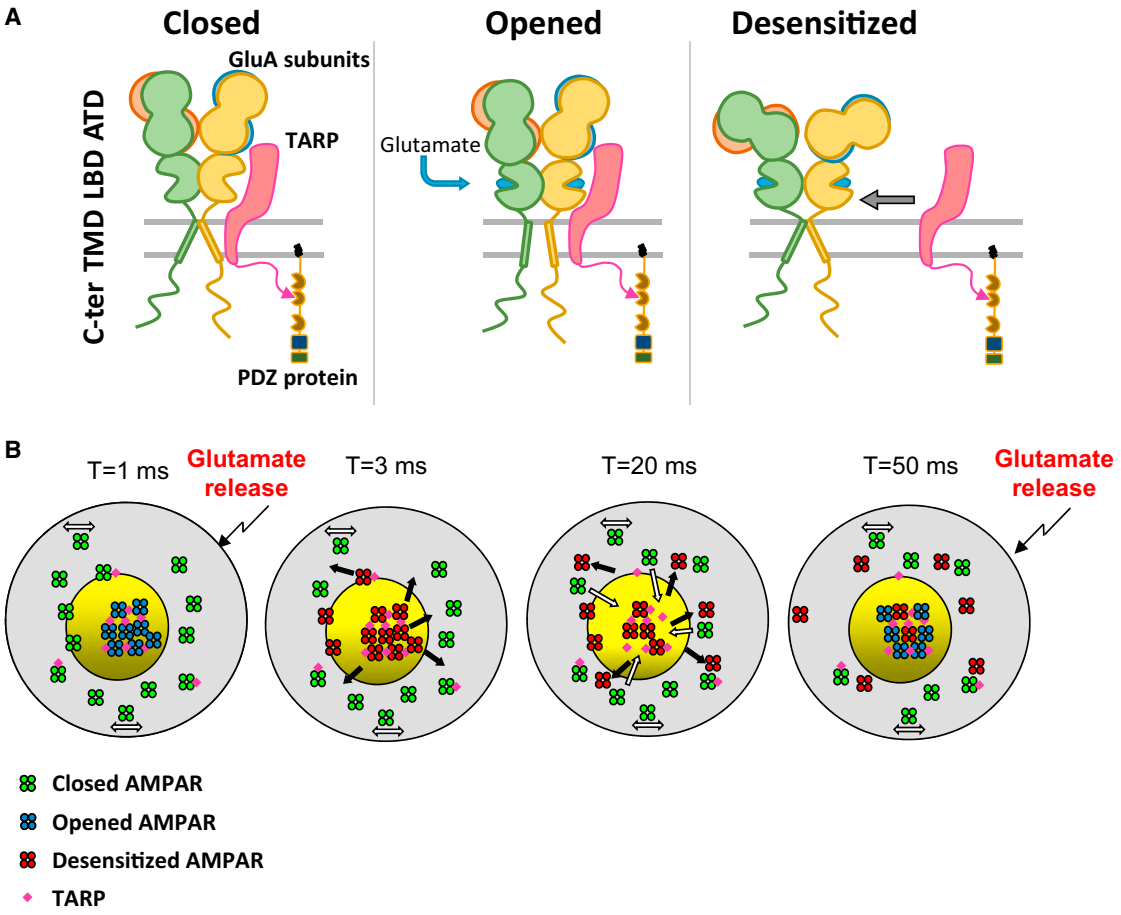

Figure 8. Hypothetical Model of Glutamate-Induced AMPAR Mobility and Effect on Synaptic Organization

(A) AMPAR are tightly coassembled with TARP at least via its transmembrane (TMD) and ligand-binding domain (LBD); the drastic changes operating at the LBD and ATD in the presence of glutamate lead to the desensitization of the AMPAR and to a decrease of its avidity for TARP. This effect could trigger a detrapping of AMPAR and an increase of its mobility.

(B) The schemes represent a top view of a synapse where naive (closed-green) AMPAR are regrouped partly in a nanocluster. The first glutamate release activates AMPAR during the first ms (T = 1 ms, blue, synaptic area covered by glutamate represented by yellow circle), then they quickly desensitize (T = 3 ms, red). This conformational change triggers an increase of AMPAR mobility, freeing TARP immobilization site. Free diffusive closed receptor can be specifically trapped at this free site (T = 20 ms), allowing a renewing of AMPAR in the nanocluster (T = 50 ms). Desensitized receptors are now out of the release site, and closed receptors replace them inside the nanocluster. This specific glutamate-induced mobility of desensitized AMPAR can be at the base of the constant receptor turnover essential for fidelity of fast synaptic transmission.

receptors within each nanodomain, it is conceivable that receptors at the center of the domain resensitize before they have the opportunity to escape the domain due to steric hindrance.

Physiological Consequences of the Enhanced AMPAR Diffusion upon Desensitization

AMPAR fast diffusion in and out of synapses allows faster recovery from desensitization-dependent paired-pulse depression for stimulation frequencies between 10 and 100 Hz (Frischknecht et al., 2009; Heine et al., 2008). All processes accelerating AMPAR diffusion increase recovery from paired-pulse depression by favoring stochastic exchange of desensitized receptors by naive ones. It was tempting to speculate that the mechanism would be even more efficient if desensitized AMPAR would escape faster from the postsynapse than naive ones.

In parallel, recent work (MacGillavry et al., 2013; Nair et al., 2013) demonstrated that around half of AMPAR are stabilized in 80 nm diameter nanoclusters in the postsynaptic density, the other part diffusing rapidly in between them (Nair et al., 2013). Our present experiments indicate that an ~20%–30% fraction of immobile AMPAR become mobile upon glutamate binding. This percentage is similar to the fraction of receptors lost from nanodomains upon glutamate application observed in d-STORM experiments. Interestingly, this loss does not modify the overall organization of AMPAR in nanodomains. We thus postulate that the increased mobility of a fraction of desensitized AMPAR is important to accelerate their exit from immobilization sites such as nanodomains to help synapses recover faster from desensitization-dependent depression. In agreement, we found that expression of the GluA-stargazin tandem, which blocks

glutamate-induced dissociation and maintains receptors immobile, increased short-term depression. In parallel, as found previously, crosslinking wild-type surface GluA1 or GluA2 also increased short-term depression, by preventing the exchange of desensitized receptors for naive ones (Heine et al., 2008).

It was previously proposed that receptor desensitization promotes the transient dissociation of TARP-AMPA receptor complexes within a few milliseconds (Morimoto-Tomita et al., 2009) and that this process accounts for the bell-shaped curve of native AMPAR steady-state glutamate-induced current concentration-response curves, reflecting the autoinactivated concentration-response behavior. The authors postulated further that this dissociation mechanism could contribute to synaptic short-term modulation by promoting paired-pulse depression, given that stargazin tends to decrease desensitization rates (Morimoto-Tomita et al., 2009; Priel et al., 2005). This is at variance with our results with the GluA1 or GluA2 chimera that both display an increased synaptic depression. Interestingly, a recent study (Semenov et al., 2012) found that a fusion protein which links the carboxyl terminus of GluA4i to the N terminus of stargazin shows similar autoinactivation to that observed in the case of separately expressed proteins, which is also in contrast to the previous results (Morimoto-Tomita et al., 2009) where covalent linkage between GluA1 and stargazin was reported to abolish autoinactivation. The reason for these discrepancies is not clear but may originate from the differences in subunits and/or linkers used for the chimera construct.

In conclusion, we propose that the increased mobility of a fraction of desensitized AMPAR is an important process to specifically allow them to diffuse out of individual nanodomains in which they would otherwise remain locked (Figure 8). Our previous simulation work established that AMPAR in nanodomains can account for as much as 70% of EPSCs (Nair et al., 2013). As AMPAR are stable in nanodomains and highly diffusive in between them, freeing desensitized AMPAR from their anchor allows them to quickly diffuse away from the glutamate bathed area in between consecutive vesicle releases. This fast exchange between desensitized and naive receptors allows maintenance of the fidelity of synaptic responses during high-frequency stimulation (Choquet, 2010; Heine et al., 2008). Our results provide a simple explanation to the regulation of synaptic transmission observed through modulation of AMPAR mobility.

EXPERIMENTAL PROCEDURES

Molecular Biology, Biochemistry, Cell Culture, and Transfection

Cloning of plasmids and cultures of rat hippocampal neurons was performed as in Nair et al. (2013) (see Supplemental Experimental Procedures for details).

Direct Stochastic Optical Reconstruction Microscopy, uPAINT Experiments, Receptor Tracking, and Analysis

Single-molecule fluorescent spots were localized in each frame and tracked over time as in Giannone et al. (2010) and Nair et al. (2013) (see Supplemental Experimental Procedures for details).

Glutamate Uncaging and Scavenging Experiments

1-P and 2-P uncaging experiments as well as glutamate scavenging were done using an inverted motorized microscope (Nikon Ti, Japan) equipped with a 100× PL-APO objective (1.49 NA) (see Supplemental Experimental Procedures for details).

Ca^{2+} Imaging, Electrophysiological Recordings, and Crosslinking Experiments

Calcium imaging and electrophysiological recordings and receptor crosslinking were performed following Heine et al. (2008) (see Supplemental Experimental Procedures for details).

Statistics

Statistical values are given as mean ± SEM unless stated otherwise (see Supplemental Experimental Procedures for details).

Ethical Approval

All experiments were approved by the Regional Ethical Committee on Animal Experiments of Bordeaux.

SUPPLEMENTAL INFORMATION

Supplemental Information includes five figures and Supplemental Experimental Procedures and can be found with this article at http://dx.doi.org/10.1016/j.neuron.2015.01.012.

AUTHOR CONTRIBUTIONS

E.H. and D.C. conceived the study, formulated the models, and wrote the manuscript. A.C. performed most single-molecule experiments. E.H. performed part of the single-molecule experiments. A.C.P. designed and performed the electrophysiology experiments for Figures 8 and S5. B.C. performed single-molecule experiments of Figures 1E–1G, S1B, S1C, 2B, and 2C. E.T. and S.M. set up and performed uncaging experiments and associated electrophysiology. N.R. performed most molecular biology constructs. A.-S.H. performed control FRET experiments. A.P. and F.C. performed immunoprecipitation experiments. All authors contributed to the preparation of the manuscript.

ACKNOWLEDGMENTS

We acknowledge C. Mulle, S. Tomita, and S. Okabe for the gift of plasmids; E. Gouaux for the anti-GluA2 antibody; J.-B. Sibarita for providing single-particle analysis software; M. Mondin at the Bordeaux Imaging Center, part of the FranceBioImaging national infrastructure, for support in microscopy; M. Sainlos and I. Gauthereau for anti-GFP nanobody production; and B. Tessier, D. Bouchet, C. Breillat, E. Verdier, and C. Genuer for cell culture and plasmid production. This work was supported by funding from ANR NanoDom and Stim-Traf-Park, Labex BRAIN and ANR-10-INBS-04 FranceBioImaging, Centre National de la Recherche Scientifique, ERC grant nanodyn-syn to D.C. and Marie Curie grant Synapsemap to A.P.

Received: February 10, 2014
Revised: November 30, 2014
Accepted: January 7, 2015
Published: February 5, 2015

REFERENCES

Armstrong, N., Sun, Y., Chen, G.Q., and Gouaux, E. (1998). Structure of a glutamate-receptor ligand-binding core in complex with kainate. Nature *395*, 913–917.

Armstrong, N., Jasti, J., Beich-Frandsen, M., and Gouaux, E. (2006). Measurement of conformational changes accompanying desensitization in an ionotropic glutamate receptor. Cell *127*, 85–97.

Ashby, M.C., Maier, S.R., Nishimune, A., and Henley, J.M. (2006). Lateral diffusion drives constitutive exchange of AMPA receptors at dendritic spines and is regulated by spine morphology. J. Neurosci. *26*, 7046–7055.

Bats, C., Groc, L., and Choquet, D. (2007). The interaction between Stargazin and PSD-95 regulates AMPA receptor surface trafficking. Neuron *53*, 719–734.

Beattie, E.C., Carroll, R.C., Yu, X., Morishita, W., Yasuda, H., von Zastrow, M., and Malenka, R.C. (2000). Regulation of AMPA receptor endocytosis by a signaling mechanism shared with LTD. Nat. Neurosci. *3*, 1291–1300.

Borgdorff, A.J., and Choquet, D. (2002). Regulation of AMPA receptor lateral movements. Nature *417*, 649–653.

Cais, O., Herguedas, B., Krol, K., Cull-Candy, S.G., Farrant, M., and Greger, I.H. (2014). Mapping the interaction sites between AMPA receptors and TARPs reveals a role for the receptor N-terminal domain in channel gating. Cell Rep. *9*, 728–740.

Choquet, D. (2010). Fast AMPAR trafficking for a high-frequency synaptic transmission. Eur. J. Neurosci. *32*, 250–260.

Choquet, D., and Triller, A. (2013). The dynamic synapse. Neuron *80*, 691–703.

Colquhoun, D., Jonas, P., and Sakmann, B. (1992). Action of brief pulses of glutamate on AMPA/kainate receptors in patches from different neurones of rat hippocampal slices. J. Physiol. *458*, 261–287.

Dürr, K.L., Chen, L., Stein, R.A., De Zorzi, R., Folea, I.M., Walz, T., Mchaourab, H.S., and Gouaux, E. (2014). Structure and dynamics of AMPA receptor GluA2 in resting, pre-open, and desensitized states. Cell *158*, 778–792.

Featherstone, D.E., and Shippy, S.A. (2008). Regulation of synaptic transmission by ambient extracellular glutamate. Neuroscientist *14*, 171–181.

Frischknecht, R., Heine, M., Perrais, D., Seidenbecher, C.I., Choquet, D., and Gundelfinger, E.D. (2009). Brain extracellular matrix affects AMPA receptor lateral mobility and short-term synaptic plasticity. Nat. Neurosci. *12*, 897–904.

Giannone, G., Hosy, E., Levet, F., Constals, A., Schulze, K., Sobolevsky, A.I., Rosconi, M.P., Gouaux, E., Tampé, R., Choquet, D., and Cognet, L. (2010). Dynamic superresolution imaging of endogenous proteins on living cells at ultra-high density. Biophys. J. *99*, 1303–1310.

Heine, M., Groc, L., Frischknecht, R., Béïque, J.C., Lounis, B., Rumbaugh, G., Huganir, R.L., Cognet, L., and Choquet, D. (2008). Surface mobility of postsynaptic AMPARs tunes synaptic transmission. Science *320*, 201–205.

Jackson, A.C., and Nicoll, R.A. (2011). The expanding social network of ionotropic glutamate receptors: TARPs and other transmembrane auxiliary subunits. Neuron *70*, 178–199.

Jin, R., Banke, T.G., Mayer, M.L., Traynelis, S.F., and Gouaux, E. (2003). Structural basis for partial agonist action at ionotropic glutamate receptors. Nat. Neurosci. *6*, 803–810.

Lin, J.W., Ju, W., Foster, K., Lee, S.H., Ahmadian, G., Wyszynski, M., Wang, Y.T., and Sheng, M. (2000). Distinct molecular mechanisms and divergent endocytotic pathways of AMPA receptor internalization. Nat. Neurosci. *3*, 1282–1290.

Lisman, J.E., Raghavachari, S., and Tsien, R.W. (2007). The sequence of events that underlie quantal transmission at central glutamatergic synapses. Nat. Rev. Neurosci. *8*, 597–609.

MacGillavry, H.D., Song, Y., Raghavachari, S., and Blanpied, T.A. (2013). Nanoscale scaffolding domains within the postsynaptic density concentrate synaptic AMPA receptors. Neuron *78*, 615–622.

Masugi-Tokita, M., and Shigemoto, R. (2007). High-resolution quantitative visualization of glutamate and GABA receptors at central synapses. Curr. Opin. Neurobiol. *17*, 387–393.

Meyerson, J.R., Kumar, J., Chittori, S., Rao, P., Pierson, J., Bartesaghi, A., Mayer, M.L., and Subramaniam, S. (2014). Structural mechanism of glutamate receptor activation and desensitization. Nature *514*, 328–334.

Morimoto-Tomita, M., Zhang, W., Straub, C., Cho, C.H., Kim, K.S., Howe, J.R., and Tomita, S. (2009). Autoinactivation of neuronal AMPA receptors via glutamate-regulated TARP interaction. Neuron *61*, 101–112.

Nair, D., Hosy, E., Petersen, J.D., Constals, A., Giannone, G., Choquet, D., and Sibarita, J.B. (2013). Super-resolution imaging reveals that AMPA receptors inside synapses are dynamically organized in nanodomains regulated by PSD95. J. Neurosci. *33*, 13204–13224.

Nakagawa, T., Cheng, Y., Ramm, E., Sheng, M., and Walz, T. (2005). Structure and different conformational states of native AMPA receptor complexes. Nature *433*, 545–549.

Opazo, P., Labrecque, S., Tigaret, C.M., Frouin, A., Wiseman, P.W., De Koninck, P., and Choquet, D. (2010). CaMKII triggers the diffusional trapping of surface AMPARs through phosphorylation of stargazin. Neuron *67*, 239–252.

Petzoldt, A.G., Lee, Y.H., Khorramshahi, O., Reynolds, E., Plested, A.J., Herzel, H., and Sigrist, S.J. (2014). Gating characteristics control glutamate receptor distribution and trafficking in vivo. Curr. Biol. *24*, 2059–2065.

Plested, A.J., and Mayer, M.L. (2009). AMPA receptor ligand binding domain mobility revealed by functional cross linking. J. Neurosci. *29*, 11912–11923.

Priel, A., Kolleker, A., Ayalon, G., Gillor, M., Osten, P., and Stern-Bach, Y. (2005). Stargazin reduces desensitization and slows deactivation of the AMPA-type glutamate receptors. J. Neurosci. *25*, 2682–2686.

Robert, A., Armstrong, N., Gouaux, J.E., and Howe, J.R. (2005). AMPA receptor binding cleft mutations that alter affinity, efficacy, and recovery from desensitization. J. Neurosci. *25*, 3752–3762.

Schnell, E., Sizemore, M., Karimzadegan, S., Chen, L., Bredt, D.S., and Nicoll, R.A. (2002). Direct interactions between PSD-95 and stargazin control synaptic AMPA receptor number. Proc. Natl. Acad. Sci. USA *99*, 13902–13907.

Schwenk, J., Harmel, N., Brechet, A., Zolles, G., Berkefeld, H., Müller, C.S., Bildl, W., Baehrens, D., Hüber, B., Kulik, A., et al. (2012). High-resolution proteomics unravel architecture and molecular diversity of native AMPA receptor complexes. Neuron *74*, 621–633.

Semenov, A., Möykkynen, T., Coleman, S.K., Korpi, E.R., and Keinänen, K. (2012). Autoinactivation of the stargazin-AMPA receptor complex: subunit-dependency and independence from physical dissociation. PLoS ONE *7*, e49282.

Shepherd, J.D., and Huganir, R.L. (2007). The cell biology of synaptic plasticity: AMPA receptor trafficking. Annu. Rev. Cell Dev. Biol. *23*, 613–643.

Sobolevsky, A.I., Rosconi, M.P., and Gouaux, E. (2009). X-ray structure, symmetry and mechanism of an AMPA-subtype glutamate receptor. Nature *462*, 745–756.

Stern-Bach, Y., Russo, S., Neuman, M., and Rosenmund, C. (1998). A point mutation in the glutamate binding site blocks desensitization of AMPA receptors. Neuron *21*, 907–918.

Sumioka, A., Yan, D., and Tomita, S. (2010). TARP phosphorylation regulates synaptic AMPA receptors through lipid bilayers. Neuron *66*, 755–767.

Sun, Y., Olson, R., Horning, M., Armstrong, N., Mayer, M., and Gouaux, E. (2002). Mechanism of glutamate receptor desensitization. Nature *417*, 245–253.

Tardin, C., Cognet, L., Bats, C., Lounis, B., and Choquet, D. (2003). Direct imaging of lateral movements of AMPA receptors inside synapses. EMBO J. *22*, 4656–4665.

Tomita, S., Fukata, M., Nicoll, R.A., and Bredt, D.S. (2004). Dynamic interaction of stargazin-like TARPs with cycling AMPA receptors at synapses. Science *303*, 1508–1511.

Tomita, S., Adesnik, H., Sekiguchi, M., Zhang, W., Wada, K., Howe, J.R., Nicoll, R.A., and Bredt, D.S. (2005a). Stargazin modulates AMPA receptor gating and trafficking by distinct domains. Nature *435*, 1052–1058.

Tomita, S., Stein, V., Stocker, T.J., Nicoll, R.A., and Bredt, D.S. (2005b). Bidirectional synaptic plasticity regulated by phosphorylation of stargazin-like TARPs. Neuron *45*, 269–277.

Traynelis, S.F., Wollmuth, L.P., McBain, C.J., Menniti, F.S., Vance, K.M., Ogden, K.K., Hansen, K.B., Yuan, H., Myers, S.J., and Dingledine, R. (2010). Glutamate receptor ion channels: structure, regulation, and function. Pharmacol. Rev. *62*, 405–496.

Turetsky, D., Garringer, E., and Patneau, D.K. (2005). Stargazin modulates native AMPA receptor functional properties by two distinct mechanisms. J. Neurosci. *25*, 7438–7448.